Supplement of Clim. Past, 16, 1411–1428, 2020
https://doi.org/10.5194/cp-16-1411-2020-supplement

Climate of the Past
Open Access

Supplement of

Comparison of observed borehole temperatures in Antarctica with simulations using a forward model driven by climate model outputs covering the past millennium

Zhiqiang Lyu et al.

Correspondence to: Zhiqiang Lyu (zhiqiang.lyu@student.uclouvain.be)

S1: Forward model description

The equation ruling subsurface temperature evolution in the forward model is given in Eq. 1. According to the original publications, we applied different methods to determine the density profile for each borehole in the model. For WAIS and Styx, the density profiles, $\rho(z)$, were obtained by a quadratic fit to the measured bulk density data following Severinghaus et al. (2010). For Larissa, the density profile was approximated following Salamatin (2000). For Mill Island, because of the similarity between the density profiles at Mill Island and Law Dome (van Ommen et al., 1999), the density is described by a piecewise exponential plus linear or dual exponential according to the analysis on the Law Dome ice core density profile (van Ommen et al., 1999). The density is considered to be constant in time in the model.

For the other parameters in the forward model, the specific heat capacity c_p is calculated by c_p = 152.5+7.122T (J kg^{-1} K^{-1}) (Cuffey and Paterson, 2010, Chap. 9, Eq. 9.1 where T is the temperature). The thermal conductivity in ice is taken from $K_{ice} = 9.828 \exp(-5.7 \times 10^{-3} T)$ (Wm^{-1}K^{-1}) (Cuffey and Paterson, 2010, Chap. 9, Eq. 9.2), and the thermal conductivity of the firn is calculated by Schwerdtfeger formula (Cuffey and Paterson, 2010, Chap. 9, Eq. 9.4). The vertical velocity at the surface is simply the accumulation rate and decreases with depth as the integral of the densification process (compaction) and the strain due to ice flow divergence. The vertical velocity profile is determined by the method of Alley et al. (1990) and Cuffey et al. (1994) with a constant strain rate. For the accumulation rate, we use a constant value derived from their original publication, which is specified in the Table 3 of the main text. The bottom boundary condition is given by the basal heat flux and the basal temperature. The heat flux is determined by matching the slope of the temperature increase in the bottom section of the record. At Mill Island, this was not possible, because the data do not extend very deep with respect to the total ice thickness. A zero heat flux boundary condition was chosen instead. The validity of this hypothesis is demonstrated in the original study of Roberts et al. (2013). The basal temperature is determined using the lower "undisturbed" sections of the measured borehole temperature extrapolated to the bottom.

In order to save computation time, the vertical discretization of the model is not homogenous. For WAIS, which is the only very deep borehole, the vertical step is of 1 m for the upper 500 m and up to 25 m for the deepest part. For other sites where the depth of borehole is close or less than 500 m, the step is set to 1 m for the whole depth range.

Before the forward model is driven by the climate model results, it is initialized with a stationary profile, which is generated after a 20000-year model run with a constant climate history and a realistic seasonal cycle. Seasonal-scale variations are "undetectable below a depth of 20m" (Cuffey and Paterson, 2010), and its does not change throughout the run. At WAIS and Styx, the seasonal cycles are determined from weather station data; at Larissa and Mill Island, since the original studies do not give the seasonal cycle, we use a seasonal cycle amplitude of 10 °C similar to WAIS (Eq. S1). At WAIS, it includes a periodic function with annual and semi-annual components, fitted to 3 years of weather station data from WAIS Divide and Byrd station (AMRC, SSEC, UW-Madison) as follows (Orsi et al., 2012):

$$T(t) = 10(\cos(2\pi t) + 0.3\cos(4\pi t)) \text{ (in K)} \qquad \text{(S1)}$$

At Styx, the seasonal cycle is determined by fitting a sinusoidal function to the automated weather station data as follows (Yang et al., 2018):

$$T(t) = 10(\cos(2\pi t) + 0.35\cos(4\pi t)) \text{ (in K)} \qquad \text{(S2)}$$

Where t is time, T is the temperature.

Equations S1 and S2 for WAIS and STYX are nearly identical, so we presume the seasonal cycle is also similar at Larissa and Mill Island, where no seasonal data is available. Including a seasonal cycle wave is important because the heat capacity and thermal conductivity depend on temperature, and temperature changes a lot in the top 15m, but below that, it is of negligible effect.

S2: Supplementary figures

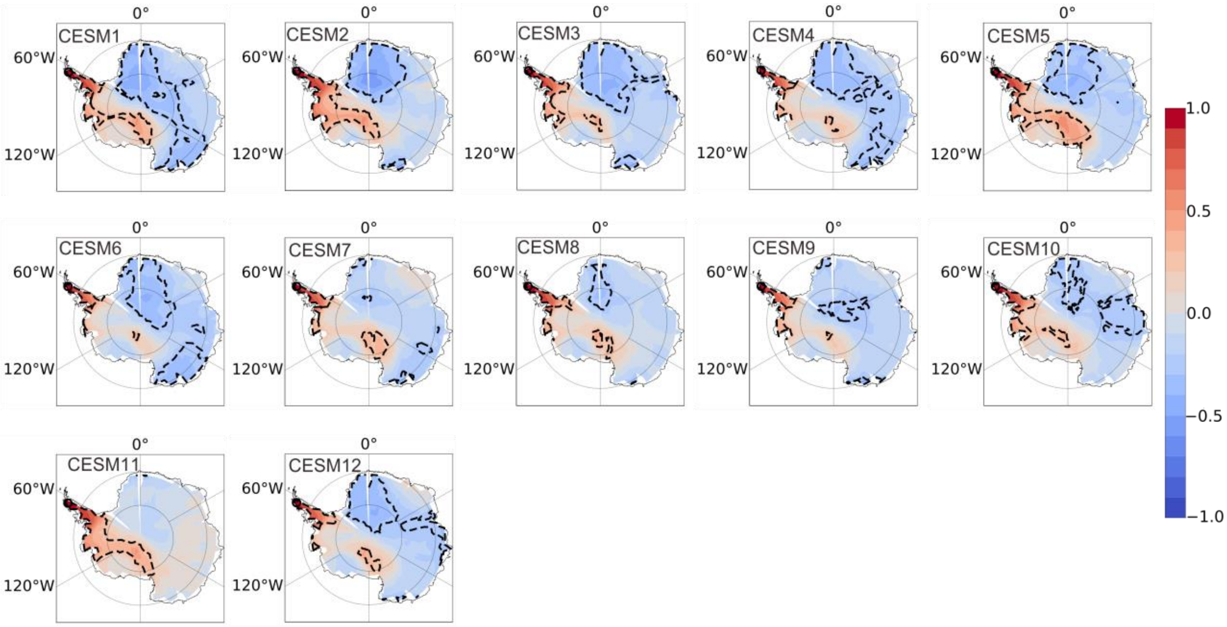

Figure S1. The correlation map (blue-red shading area) showing the relationship between the temperature from 1825 to 1925 CE at Larissa and other grid cells in Antarctica for each CESM member. The black dotted contour lines show a significant correlation at the 99 % significant level.

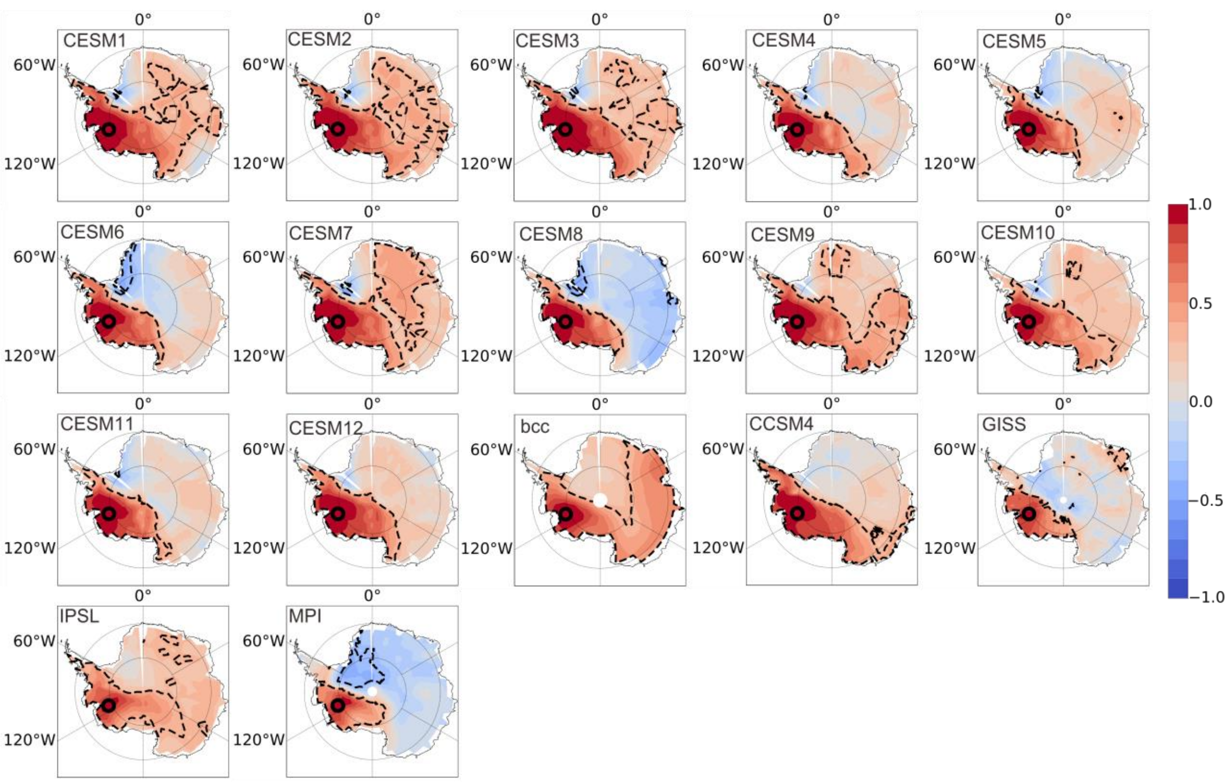

Figure S2. The correlation map showing the relationship between the temperature from 1950 to 2005 CE at WAIS and other grid cells for each climate models. The red dashed contour lines show a significant correlation at the 99% significant level.

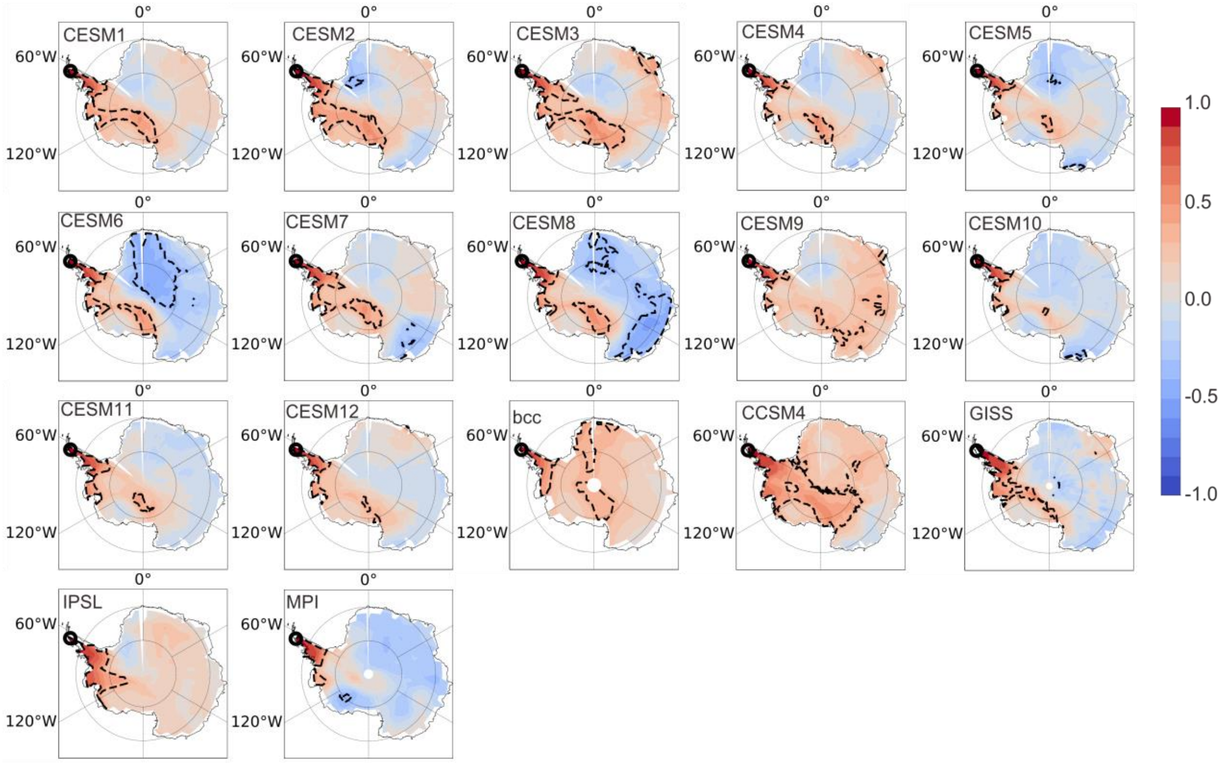

Figure S3. The correlation map showing the relationship between the temperature from 1950 to 2005 CE at Larissa and other grid cells for each climate models. The red dashed contour lines show a significant correlation at the 99% significant level.

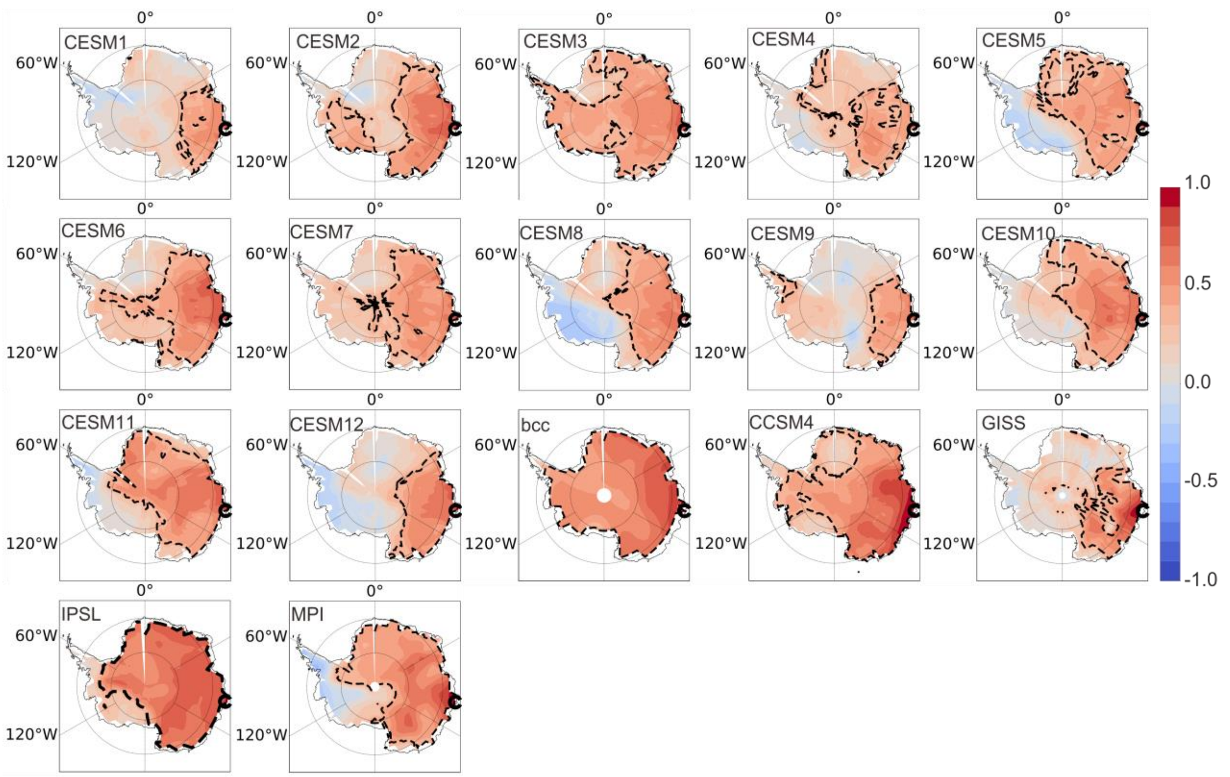

Figure S4. The correlation map showing the relationship between the temperature from 1950 to 2005 CE at Mill Island and other grid cells for each climate models. The red dashed contour lines show a significant correlation at the 99% significant level.

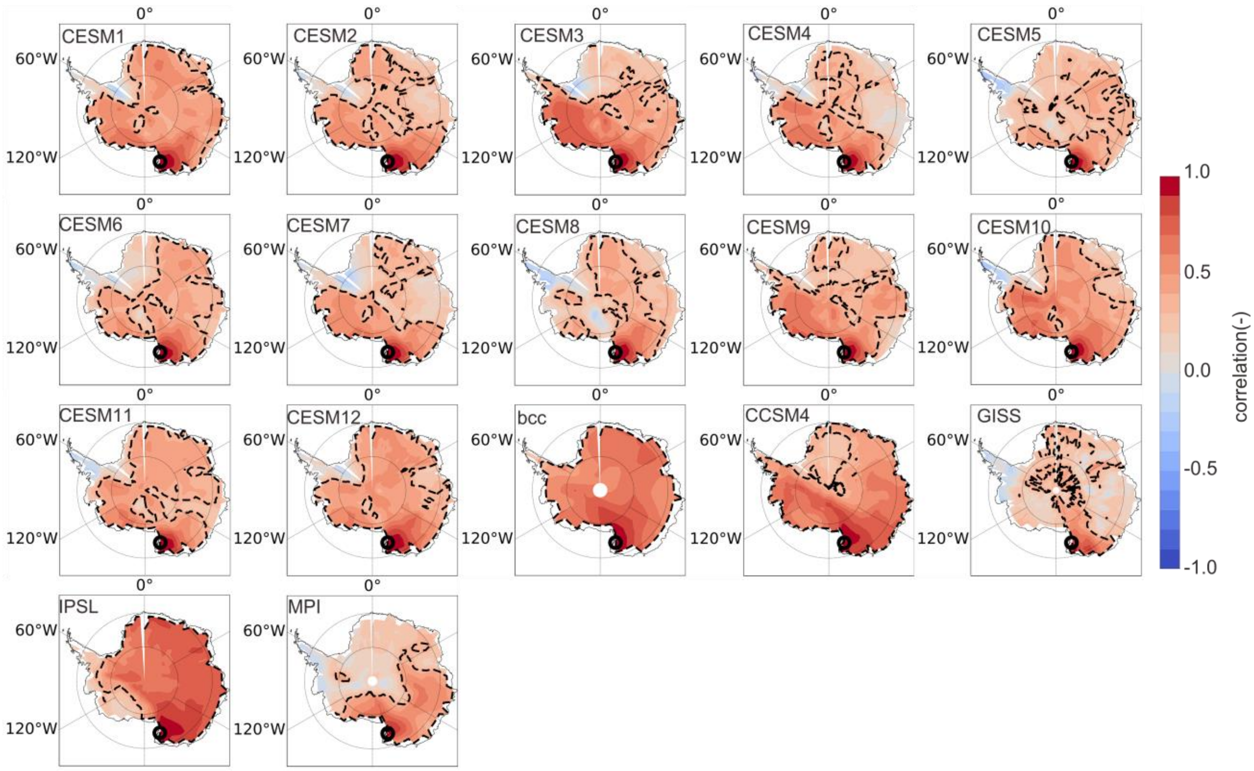

Figure S5. The correlation map showing the relationship between the temperature from 1950 to 2005 CE at Styx and other grid cells for each climate models. The red dashed contour lines show a significant correlation at the 99% significant level.

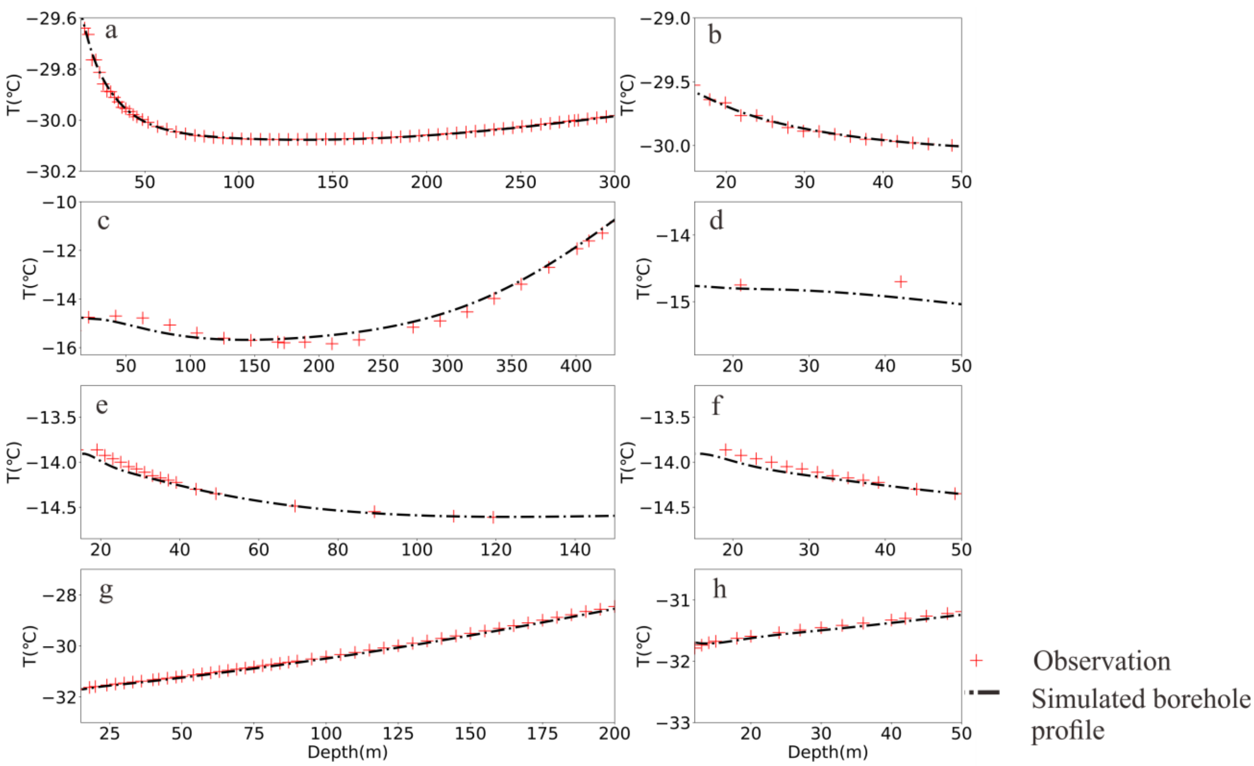

Figure S6. Comparison of borehole temperature profile outputs for the forward model driven by the corresponding reconstruction with the observation at each site. (a) WAIS: 15-300 m; (b) WAIS: 15-50 m; (c) Larissa: 15-430 m; (d) Larissa:15-50 m; (e) Mill Island:15-150 m; (f) Mill Island:15-50 m; (g) Styx:15-200 m; (h) Styx:15-50 m. The thick dash-dot line denotes the simulated borehole profile at each site, and red across represent the observation.

S3: Observed borehole temperature distribution at WAIS.

Depth(m)	Temperature (°C)
7.96	-29.7594
9.19	-29.604
9.95	-29.5588
11.94	-29.4741
13.93	-29.4806
15.92	-29.5267
17.91	-29.6397
19.9	-29.6645
21.89	-29.7642
23.89	-29.7642
25.88	-29.8132
27.87	-29.8587
29.86	-29.8871
31.85	-29.8891
33.84	-29.9115
35.83	-29.9285
37.82	-29.9503
39.81	-29.9549
41.8	-29.9663
43.79	-29.9785
45.78	-29.9872
48.77	-29.998
51.75	-30.0089
56.73	-30.0253
61.7	-30.0352
66.68	-30.046
71.65	-30.0538
76.63	-30.0603
81.6	-30.0635
86.58	-30.0682
91.55	-30.0701
96.53	-30.0724
101.5	-30.0738
106.48	-30.0746
111.55	-30.0753
116.43	-30.0755
121.4	-30.0757
126.38	-30.0756
131.35	-30.0753
136.33	-30.0752
141.3	-30.0748

146.28	-30.0743
151.25	-30.0736
156.23	-30.0734
161.2	-30.0722
166.18	-30.0715
171.15	-30.0698
176.13	-30.0686
181.1	-30.0672
186.08	-30.0653
191.05	-30.0632
196.03	-30.0608
201	-30.0584
205.98	-30.0564
210.95	-30.0532
215.93	-30.0502
220.9	-30.0471
225.88	-30.0436
230.85	-30.0404
235.83	-30.0365
240.8	-30.0329
245.78	-30.0299
250.75	-30.0248
255.73	-30.022
260.7	-30.0165
265.68	-30.0129
270.65	-30.0078
275.63	-30.0042
278.61	-30.0017
280.6	-30.0003
285.58	-29.9954
290.55	-29.991
295.53	-29.9863
300.5	-29.9821

S4: Observed borehole temperature distribution at LARISSA.

Depth(m)	Temperature (°C)
8.41	-15.35
10.51	-15.3
21.02	-14.75
42.04	-14.7
63.06	-14.78
84.09	-15.07
105.11	-15.4

126.13	-15.61
147.15	-15.7
168.17	-15.77
173	-15.8
189.19	-15.77
210.21	-15.84
231.24	-15.68
273.28	-15.16
294.3	-14.9
315.32	-14.53
336.34	-13.98
357.36	-13.39
378.86	-12.7
400.77	-11.93
409.92	-11.61
420.43	-11.29
430.94	-10.82

S5: Observed borehole temperature distribution at Mill Island.

Depth(m)	Temperature (°C)
9.05	-14.275
14.06	-13.8625
19.07	-13.8625
21.07	-13.925
23.07	-13.9625
25.07	-14
27.07	-14.05
29.07	-14.075
31.09	-14.1125
33.09	-14.15
35.11	-14.175
37.11	-14.2
39.11	-14.225
44.125	-14.3
49.14	-14.35
69.17	-14.4875
89.24	-14.55
109.3	-14.6
119.31	-14.6125

S6: Observed borehole temperature distribution at Styx.

Depth(m)	Temperature (°C)
1	-29.7244
2	-32.6116
3	-33.4131
4	-33.522

5	-33.2036
6	-32.9317
7	-32.5716
8	-32.3349
9	-32.1212
10	-31.9562
11	-31.8512
12	-31.7853
13	-31.7379
14	-31.6974
15	-31.6752
18	-31.6255
20	-31.5921
24	-31.5332
27	-31.4905
30	-31.452
33	-31.4144
36	-31.3781
40	-31.3275
42	-31.3006
45	-31.2628
48	-31.2209
50	-31.1898
54	-31.1366
57	-31.0925
60	-31.0493
63	-31.0032
66	-30.9585
69	-30.9144
72	-30.8683
75	-30.82
78	-30.7722
81	-30.7296
84	-30.6835
87	-30.6367
90	-30.5892
95	-30.5113
100	-30.4264
105	-30.3411
110	-30.253
115	-30.1648
120	-30.081
125	-29.9906
130	-29.8973
135	-29.803
140	-29.7075
145	-29.6079
150	-29.5078

155	-29.412
160	-29.3098
165	-29.2065
170	-29.0968
175	-28.9922
180	-28.883
185	-28.7783
190	-28.6518
195	-28.5633
200	-28.4535
205	-28.3431
210	-28.2515

Reference

Alley, R. B., and Koci, B. R.: Recent Warming in Central Greenland?, Ann. Glaciol., 14, 6-8, https://doi.org/10.3189/s0260305500008144, 1990.

Cuffey, K. M., Alley, R. B., Grootes, P. M., Bolzan, J. M., and Anandakrishnan, S.: Calibration of the $\delta^{18}O$ isotopic paleothermometer for central Greenland, using borehole temperatures, Journal of Glaciology, 40, 341-349, 10.3189/s0022143000007425, 1994.

Cuffey, K., and W. Paterson, The Physics of Glaciers, Academic, Amsterdam, 2010.

Orsi, A. J., Cornuelle, B. D., and Severinghaus, J. P.: Little Ice Age cold interval in West Antarctica: Evidence from borehole temperature at the West Antarctic Ice Sheet (WAIS) Divide, Geophys. Res. Lett., 39, https://doi.org/10.1029/2012gl051260, 2012.

Roberts, J. L., Moy, A. D., van Ommen, T. D., Curran, M. A. J., Worby, A. P., Goodwin, I. D., and Inoue, M.: Borehole temperatures reveal a changed energy budget at Mill Island, East Antarctica, over recent decades, Cryosphere, 7, 263-273, https://doi.org/10.5194/tc-7-263-2013, 2013.

Salamatin A. N.: Paleoclimatic reconstructions based on borehole temperature measurements in ice sheets. Possibilities and limitations, in: Physics of Ice Core Records, edited by: Hondoh, T., Hokkaido University Press, Sapporo, 243–282, 2000.

Severinghaus, J.P., Albert, M.R., Courville, Z.R., Fahnestock, M.A., Kawamura, K., Montzka, S.A., Mühle, J., Scambos, T.A., Shields, E., Shuman, C.A. and Suwa, M.: Deep air convection in the firn at a zero-accumulation site, central Antarctica, Earth Planet. Sci. Lett., 293(3-4), 359-367, https://doi.org/10.1016/j.epsl.2010.03.003, 2010.

van Ommen, T., Morgan, V., Jacka, T., Woon, S., and Elcheikh, A.: Near-surface temperatures in the Dome Summit South (Law Dome, East Antarctica) borehole, Ann. Glaciol., 29, 141–144, https://doi.org/10.3189/172756499781821382 ,1999.

Yang, J.-W., Han, Y., Orsi, A. J., Kim, S.-J., Han, H., Ryu, Y., Jang, Y., Moon, J., Choi, T., Hur, S. D., and Ahn, J.: Surface Temperature in Twentieth Century at the Styx Glacier, Northern Victoria Land, Antarctica, From Borehole Thermometry, Geophys. Res. Lett., 45, 9834-9842, https://doi.org/10.1029/2018gl078770, 2018.